

Study of the radiative decay $J/\psi \rightarrow \gamma \rho \rho$

R. M. Baltrusaitis,^(a) D. Coffman, J. Hauser, D. G. Hitlin, J. D. Richman,^(b)
J. J. Russell,^(c) and R. H. Schindler

California Institute of Technology, Pasadena, California 91125

D. E. Dorfan, R. Fabrizio,^(d) F. Grancagnolo,^(b) R. P. Hamilton,^(e) C. A. Heusch,
L. Köpke, R. Partridge, J. Perrier, H. F. W. Sadrozinski, M. Scarlatella, T. L. Schalk, and A. Seiden
University of California at Santa Cruz, Santa Cruz, California 95064

J. J. Becker,^(f) G. T. Blaylock, J. S. Brown, H. Cui,^(g) B. I. Eisenstein, G. Gladding,
S. A. Plaetzer, A. L. Spadafora,^(h) J. J. Thaler, A. Wattenberg, and W. J. Wisniewski
University of Illinois at Urbana-Champaign, Urbana, Illinois 61801

K. O. Bunnell, R. E. Cassell, D. H. Coward, K. F. Einsweiler,^(b) L. Moss, R. F. Mozley, A. Odian,
J. R. Roehrig,⁽ⁱ⁾ W. Toki, Y. Unno,^(j) F. Villa, N. Vermes, D. Wisinski, and G. Wolf
Stanford Linear Accelerator Center, Stanford, California 94305

T. H. Burnett, V. Cook, C. Del Papa,^(b) A. L. Duncan, P. M. Mockett, A. Nappi,^(k)
J. C. Sleeman,^(l) and H. J. Willutzki

University of Washington, Seattle, Washington 98195

(Mark III Collaboration)

(Received 29 July 1985)

We present an analysis of the decay $J/\psi \rightarrow \gamma 4\pi$ in the final states $\gamma \pi^+ \pi^- \pi^+ \pi^-$ and $\gamma \pi^+ \pi^0 \pi^- \pi^0$. The branching fractions obtained are $B(J/\psi \rightarrow \gamma \pi^+ \pi^- \pi^+ \pi^-) = (3.05 \pm 0.08 \pm 0.45) \times 10^{-3}$ and $B(J/\psi \rightarrow \gamma \pi^+ \pi^0 \pi^- \pi^0) = (8.3 \pm 0.2 \pm 3.1) \times 10^{-3}$ for $m_{4\pi}$ less than $2 \text{ GeV}/c^2$. The 4π invariant-mass distributions extend from 1.0 to $3.0 \text{ GeV}/c^2$, showing peaks at approximately 1.55 and $1.8 \text{ GeV}/c^2$. In an analysis of the 4π final state we find that $\approx 50\%$ of the events below $2 \text{ GeV}/c^2$ are pseudoscalar $\rho\rho$, the product branching fraction of which is determined to be $B(\psi \rightarrow \gamma X_0) B(X_0 \rightarrow \rho\rho) = (4.7 \pm 0.3 \pm 0.9) \times 10^{-3}$. No other significant $\rho\rho$ component is found, and upper limits on the product branching fraction $B(J/\psi \rightarrow \gamma X) B(X \rightarrow \rho\rho)$ are presented for the $\theta(1690)$ and the g_T states near $2.2 \text{ GeV}/c^2$.

I. INTRODUCTION

Radiative decays of the J/ψ to states other than the η_c are believed to proceed via a two-gluon intermediate state¹ and are thus an excellent place to look for gluon-gluon bound states, or glueballs, expected from QCD. Since quark-antiquark states are observed in J/ψ radiative decays as well, the physical final states are expected to be mixtures of quark and gluon bound states such as $q\bar{q}$, gg , and perhaps $q\bar{q}g$ and $qq\bar{q}\bar{q}$. In what follows, however, we shall follow current usage, referring to such states as glueballs, while cognizant of their likely mixed character. A large J/ψ radiative coupling could be indicative of a large glueball component.

Two states found in J/ψ radiative decays do not seem to fit into $q\bar{q}$ nonets. These are the pseudoscalar meson $\iota(1440)$ (Refs. 2 and 3) and the tensor meson $\theta(1690)$ (Refs. 4 and 5). They are thus viewed as glueball candidates. The three 2^{++} states $g_T(2120)$, $g_T(2200)$, and $g_T(2360)$, observed in $\pi^- p$ interactions,⁶ have been interpreted as glueballs, but they have not been observed in radiative J/ψ decays. Since these states were found to decay to $\phi\phi$, from flavor symmetry one might expect com-

parable $\rho\rho$ decay branching fractions.

The decay $J/\psi \rightarrow \gamma \rho^0 \rho^0$ was first observed by Mark II (Ref. 7). The $\rho\rho$ mass distribution was found to be concentrated below $2 \text{ GeV}/c^2$ with structure near $1.65 \text{ GeV}/c^2$. Several authors⁸ have pointed out that if this structure was due to the $\theta(1690)$, the branching fraction for $J/\psi \rightarrow \gamma \theta(1690)$ would be $\approx 5 \times 10^{-3}$, a factor of 3 larger than that observed for $\eta\eta$ and $K\bar{K}$ final states, which would make a glueball interpretation of this state more likely.

Enhancements in $\rho\rho$ final states with masses below $2 \text{ GeV}/c^2$ have also been found in hadronic interactions⁹ and in photon-photon collisions.¹⁰ Interpretations of these enhancements include resonance production of $q\bar{q}$, $qq\bar{q}\bar{q}$, $q\bar{q}g$, and gg bound states. Because the observation of large $\rho\rho$ production cross sections near threshold in $\gamma\gamma$ collisions and radiative J/ψ decays bear some similarity, it has been proposed¹¹ that the underlying dynamics has the same origin. A spin-parity analysis¹² of $\gamma\gamma \rightarrow \rho^0 \rho^0$ indicates that the $\rho\rho$ system is mostly 0^+ below $1.7 \text{ GeV}/c^2$ and mostly 2^+ above, but cannot rule out an isotropic model. Negative parity, however, is excluded by the analysis.

This paper presents results from an analysis of the decays $J/\psi \rightarrow \gamma\pi^+\pi^-\pi^+\pi^-$ and $J/\psi \rightarrow \gamma\pi^+\pi^0\pi^-\pi^0$, $\pi^0 \rightarrow \gamma\gamma$, obtained with the Mark III detector at the SLAC storage ring SPEAR using $(2.71 \pm 0.16) \times 10^6$ J/ψ produced in e^+e^- collisions. A multichannel spin-parity analysis of the final states is employed to investigate the $\rho\rho$ component of the 4π system. Section II describes the event selection procedures and background analysis. The spin-parity analysis is described in Sec. III. Discussion of the results and conclusions are presented in Sec. IV. Details of the spin-parity analysis method are relegated to the Appendix.

II. DETECTOR AND EVENT SELECTION

The Mark III detector has been fully described elsewhere.¹³ This analysis uses information from the central cylindrical drift chamber, which measures momenta of charged tracks with a resolution of $\sigma_p/p = 2\%$ at 1 GeV/c. Tracks are accepted for which $|\cos\theta| < 0.83$, where θ is the polar angle with respect to the beam direction. Photons are reconstructed with electromagnetic shower counters, which cover 94% of the solid angle and detect photons with an energy resolution of $\sigma_E/E = 17\%/\sqrt{E}$ (GeV) and with 100% detection efficiency for energies greater than 100 MeV. Kinematically constrained fits of the exclusive final states considered here improve the resolution of the photon energy measurement. Since hadronic interactions of charged pions in the shower counters produce spurious showers that may be mistaken for primary photons, photon candidates are defined as showers outside a cone of half-angle 18° around any charged particle.

Candidates for the decay $J/\psi \rightarrow \gamma\pi^+\pi^-\pi^+\pi^-$ are selected by requiring exactly four charged tracks in the drift chamber with zero total charge. Events are required to have between one and three photons to allow for spurious signals discussed above. At least one photon is required to have an energy greater than 100 MeV and to lie within $|\cos\theta_\gamma| < 0.7$. A small background due to $K_S^0 K_S^0$ is rejected by $\pi\pi$ mass cuts ($|m_{\pi\pi} - m_{K_S^0}| > 20$ MeV/c²).

The difference between the missing energy recoiling against the four-pion system and the magnitude of the missing momentum is denoted by U . A cut of $|U| < 0.1$ GeV is required which removes events for which the invariant mass of the neutrals is greater than m_{π^0} , as well as events with charged kaons. Kinematically constrained fits [four-constraint (4C)] are applied to improve the resolution as discussed above, and also to select the radiative photon when there is more than one photon candidate in the event.

Events of the type $J/\psi \rightarrow \gamma\pi^+\pi^0\pi^-\pi^0$ are selected by requiring two oppositely charged tracks in the drift chamber and between five and seven photons. Fiducial cuts for the photons require $|\cos\theta_\gamma| < 0.80$ or $0.85 < |\cos\theta_\gamma| < 0.95$. A minimum energy of 40 MeV is required for photons. Kinematic fits (6C) are applied which include the two π^0 mass constraints. For events with more than five showers, fits are also performed to determine whether the hypothesis $J/\psi \rightarrow 5\pi$ has a smaller

χ^2 than the signal hypothesis, and if so, the candidate is rejected. The combination with the smallest χ^2 is used for further analysis. Apart from improving the resolution, the kinematic fits are used to identify the radiative photon and the photons from the π^0 decays. The quantity U can now be calculated as above using the measured momenta for the charged pions. For π^0 's the energies and momenta obtained from a 1C fit of the photon pairs to the π^0 hypothesis are used. A cut $|U| < 0.25$ GeV is imposed.

At this point a loose cut $\chi^2 < 20$ is made on both samples yielding 17933 $\gamma\pi^+\pi^-\pi^+\pi^-$ and 29341 $\gamma\pi^+\pi^0\pi^-\pi^0$ candidates. Figures 1(a) and 1(b) show the (constrained) 4π mass distributions for these events. These distributions are dominated by background from $J/\psi \rightarrow 5\pi$ where a π^0 decays asymmetrically and one of the decay photons is misinterpreted as the radiative photon. To study this background, a sample of $J/\psi \rightarrow \pi^0\pi^+\pi^-\pi^+\pi^-$ events is selected, using 5C fits and requiring that the π^0 not decay too asymmetrically, $|E_{\gamma 1} - E_{\gamma 2}|/E_{\pi^0} < 0.8$. The $\pi^+\pi^-\pi^+\pi^-$ mass distribution for these events is shown in Fig. 1(c). The overall shape of Figs. 1(a)–1(c) is similar. Structure below 2 GeV/c², however, is observed only in (a) and (b), but not in (c). The observation of the η_c decay to 4π , shown in the inset of Fig. 1(a), is reported elsewhere.¹⁴

Next the 5π background is subtracted and the remaining structures are shown to be due to the $\gamma 4\pi$ final state. The amount of background from $J/\psi \rightarrow 5\pi$ can be estimated by a technique that uses the measured direction of the radiative photon.¹⁵ The transverse momentum of the 4π system relative to that direction is defined by

$$p_{t_\gamma}^2 = 4 |\mathbf{p}_{4\pi}|^2 \sin^2(\delta/2),$$

where $\mathbf{p}_{4\pi}$ is the momentum vector of the four-pion system and δ is the angle between the radiative photon and the four-pion momentum vector. For $\gamma\pi^+\pi^-\pi^+\pi^-$ this quantity is calculated using the unconstrained measurements. For $\gamma\pi^+\pi^0\pi^-\pi^0$ the π^0 momenta are derived from 1C fits to the π^0 mass constraint. Background events from $J/\psi \rightarrow 5\pi$ with a missing photon lead to a distribution of $p_{t_\gamma}^2$ that is broad compared with the experimental resolution. Examination of $p_{t_\gamma}^2$ allows a statistical separation of radiative from nonradiative decays. Further advantages of the use of this variable are that it does not depend on the measured energy of the radiative photon, and that the resolution is nearly independent of the 4π mass. Figure 2(a) shows the $p_{t_\gamma}^2$ distribution for the $\pi^+\pi^-\pi^+\pi^-$ data sample. The shaded band is the Monte Carlo expectation for the 5π background reaction normalized in the tail of the distribution, 0.004 (GeV/c)² $\leq p_{t_\gamma}^2 \leq 0.01$ (GeV/c)², after correcting for leakage from the signal region. The dashed curve represents the Monte Carlo simulation for $\gamma 4\pi$ events, added to the background contribution. The events above the band represent the radiative signal. The uncertainty in the branching fraction introduced by the normalization procedure is less than 5%. We find 1727 ± 83 events with $p_{t_\gamma}^2 < 0.0015$ (GeV/c)² and $m_{4\pi}$ below 2 GeV/c².

The corresponding plot for $J/\psi \rightarrow \gamma\pi^+\pi^0\pi^-\pi^0$ is

shown in Fig. 2(b). The separation between the radiative and the 5π reaction is much less reliable in this case, because the background also peaks at low $p_{t\gamma}^2$. Therefore the $p_{t\gamma}^2$ distribution, as obtained from the data, is compared to Monte Carlo calculations using $\gamma 4\pi$ and 5π events generated according to phase space. The dashed curve in Fig. 2(b) is the result of a fit of the Monte Carlo-generated distributions to the data. The solid curve is the 5π portion. The number of events above this line is due to $J/\psi \rightarrow \gamma 4\pi$. The uncertainty in the branch-

ing fraction introduced in this case is 40%. There are 1104 ± 410 events with $p_{t\gamma}^2 < 0.004$ (GeV/c)² for four-pion masses less than $2 \text{ GeV}/c^2$.

Figures 3(a) and 3(b) show the four-pion mass distribution after cuts of $p_{t\gamma}^2 < 0.0015$ (GeV/c)² and $p_{t\gamma}^2 < 0.0040$ (GeV/c)², respectively, are applied. The sum of the distributions is shown in Fig. 3(c). The contributions from $J/\psi \rightarrow 5\pi$, are indicated by the shaded bands, which also display the uncertainty in the normalization of this background. The shape of the background $m_{4\pi}$ distribution is determined from a $J/\psi \rightarrow 5\pi$ phase-space Monte Carlo simulation and, in the case of the $\gamma 2(\pi^+\pi^-)$ mode, also derived from selected $\pi^0 2(\pi^+\pi^-)$ events. For the latter, Monte Carlo and data $m_{4\pi}$ distributions are in excellent agreement below $2.6 \text{ GeV}/c^2$. For $\gamma\pi^+\pi^0\pi^-\pi^0$ we assume that the shape of the background $m_{4\pi}$ distribution is also dominated by $J/\psi \rightarrow 5\pi$ phase space. Note however that the absolute magnitude of the 5π background is independent of this assumption since the estimate of its magnitude depends only on the π^0 decay properties that determine the $p_{t\gamma}^2$ distributions of Fig. 2. The subtracted distributions, which represent radiative $J/\psi \rightarrow \gamma 4\pi$, are shown in Figs. 4(a) and 4(b). Two maxima appear in all

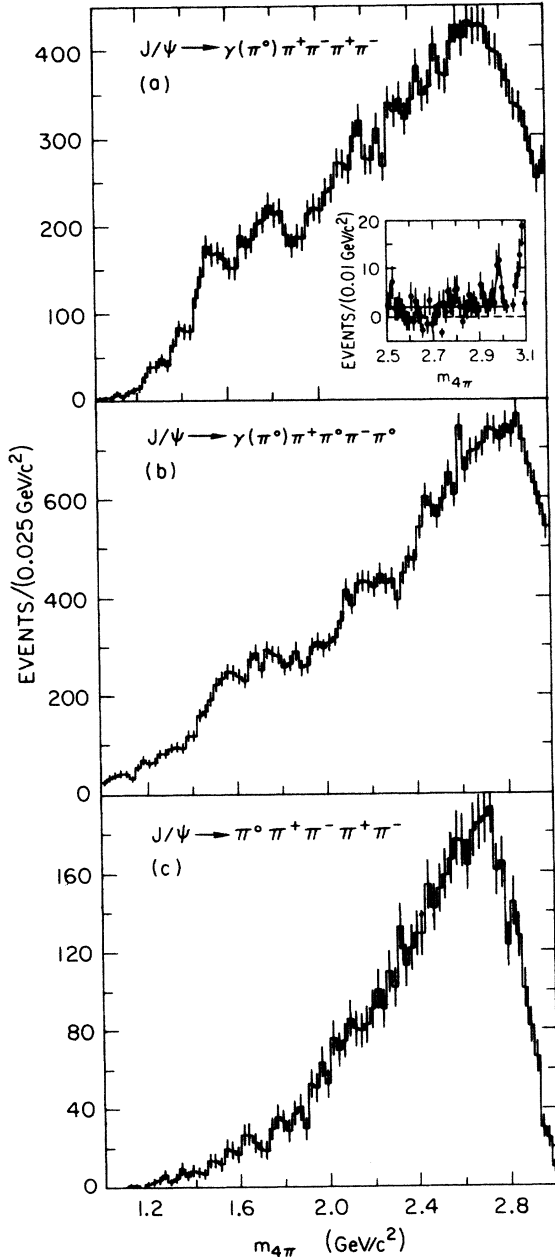


FIG. 1. (a) $m_{\pi^+\pi^-\pi^+\pi^-}$ and (b) $m_{\pi^+\pi^0\pi^-\pi^0}$ distributions after event selection. The notation $\gamma(\pi^0)$ indicates that both $\gamma 4\pi$ and 5π events are present. (c) $m_{4\pi}$ distribution from $J/\psi \rightarrow \pi^0\pi^+\pi^-\pi^+\pi^-$ events. The inset in (a) displays the region 2.5 to 3.1 GeV/c^2 in 10 MeV/c^2 bins after additional cuts (Ref. 14).

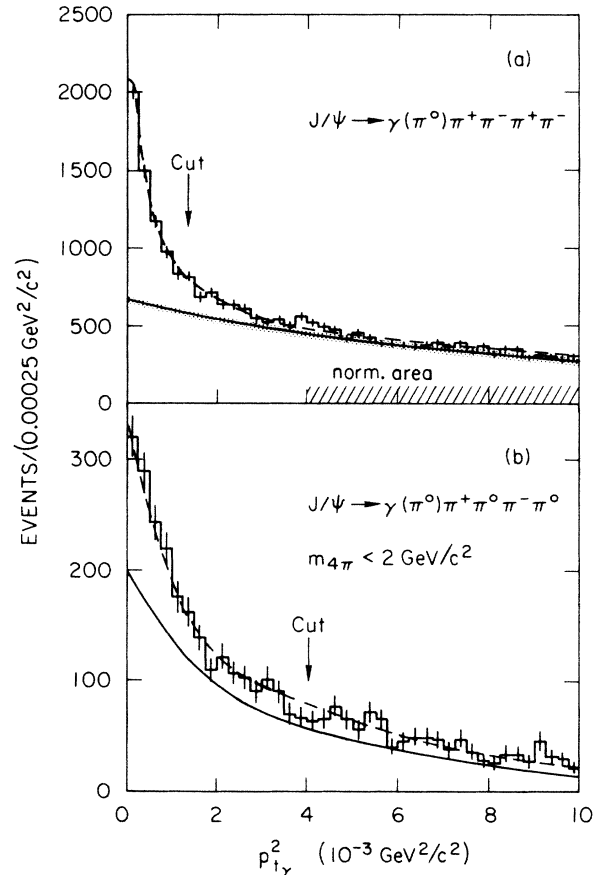


FIG. 2. $p_{t\gamma}^2$ distributions for (a) $\gamma(\pi^0)\pi^+\pi^-\pi^+\pi^-$ and (b) $\gamma(\pi^0)\pi^+\pi^0\pi^-\pi^0$ final states. The band in (a) and the solid curve in (b) are the background contribution from $J/\psi \rightarrow 5\pi$. The dashed curves are Monte Carlo calculations for $J/\psi \rightarrow \gamma 4\pi$ added to the 5π contributions.

distributions of Figs. 3 and 4 at masses of ~ 1.55 and ~ 1.8 GeV/c^2 , respectively, both approximately 0.1 GeV/c^2 wide.

A Monte Carlo simulation including all of the analysis cuts determines the detection efficiency to be 0.208 ± 0.024 for $\gamma\pi^+\pi^-\pi^+\pi^-$ and 0.049 ± 0.006 for $\gamma\pi^+\pi^0\pi^-\pi^0$, both independent of $m_{4\pi}$. This leads to branching fractions for $m_{4\pi}$ masses below 2 GeV/c^2 of

$$B(J/\psi \rightarrow \gamma\pi^+\pi^-\pi^+\pi^-) = (3.05 \pm 0.08 \pm 0.45) \times 10^{-3},$$

$$B(J/\psi \rightarrow \gamma\pi^+\pi^0\pi^-\pi^0) = (8.3 \pm 0.2 \pm 3.1) \times 10^{-3}.$$

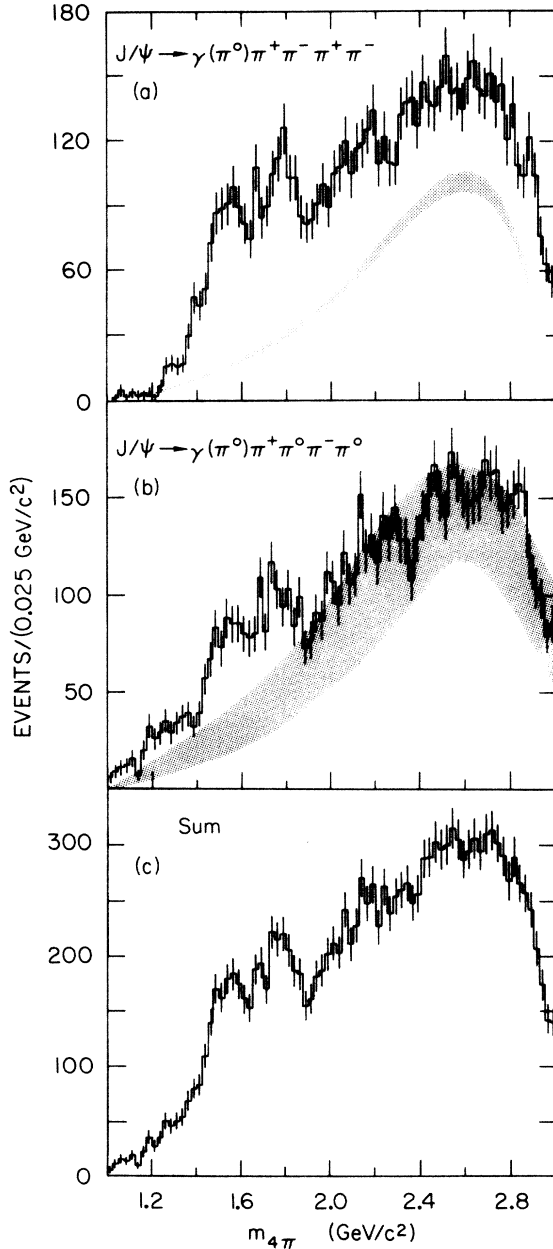


FIG. 3. $m_{4\pi}$ distributions for (a) $\pi^+\pi^-\pi^+\pi^-$ and (b) $\pi^+\pi^0\pi^-\pi^0$, for events with $p_{t,\gamma}^2 < 0.0015$ $(\text{GeV}/c)^2$ (a) and $p_{t,\gamma}^2 < 0.0040$ $(\text{GeV}/c)^2$ (b). The bands display the 5π background distribution estimated from Fig. 2. (c) is the sum of (a) and (b).

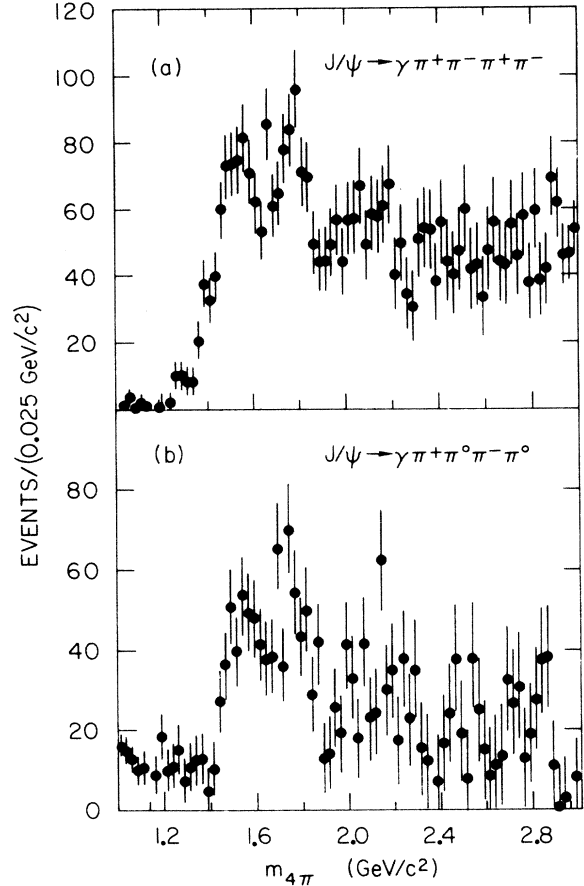


FIG. 4. Background-subtracted $m_{4\pi}$ distributions for (a) $\gamma\pi^+\pi^-\pi^+\pi^-$ and (b) $\gamma\pi^+\pi^0\pi^-\pi^0$ events obtained by subtracting the center values of the bands in Fig. 3. The uncertainty introduced by the background subtraction of (a) 5% and (b) 40% is not included in the error bars.

The ratio of the branching fractions is $B(J/\psi \rightarrow \gamma\pi^+\pi^0\pi^-\pi^0)/B(J/\psi \rightarrow \gamma\pi^+\pi^-\pi^+\pi^-) = 2.7 \pm 1.1$.

This is consistent with a value of 2 which is expected if the 4π system is isoscalar and the $\pi^+\pi^-$ ($\pi^\pm\pi^0$) systems are isovector. For the $\pi^+\pi^-\pi^+\pi^-$ mode the branching fraction for $m_{4\pi}$ less than 3 GeV/c^2 is

$$B(J/\psi \rightarrow \gamma\pi^+\pi^-\pi^+\pi^-) = (6.4 \pm 0.2 \pm 0.8) \times 10^{-3}.$$

For the remainder of this paper, the ratio of $\gamma 4\pi$ signal to 5π background is maximized. This is achieved for $J/\psi \rightarrow \gamma\pi^+\pi^-\pi^+\pi^-$ by considering only events with exactly one photon and by increasing the fiducial region for photon detection to the range used for $J/\psi \rightarrow \gamma\pi^+\pi^0\pi^-\pi^0$. For the latter at most one spurious photon outside the 18° cone around charged tracks with energy less than 80 MeV is allowed. In addition the χ^2 probability of the kinematic fits is required to be greater than 5% for both modes. These requirements are made in addition to the already existing cuts, in particular the $p_{t,\gamma}^2$ cut.

There are 4065 and 4798 events below 3 GeV/c^2 in the two samples, respectively, for which the four-pion mass distributions are shown in Fig. 5. The remaining 5π con-

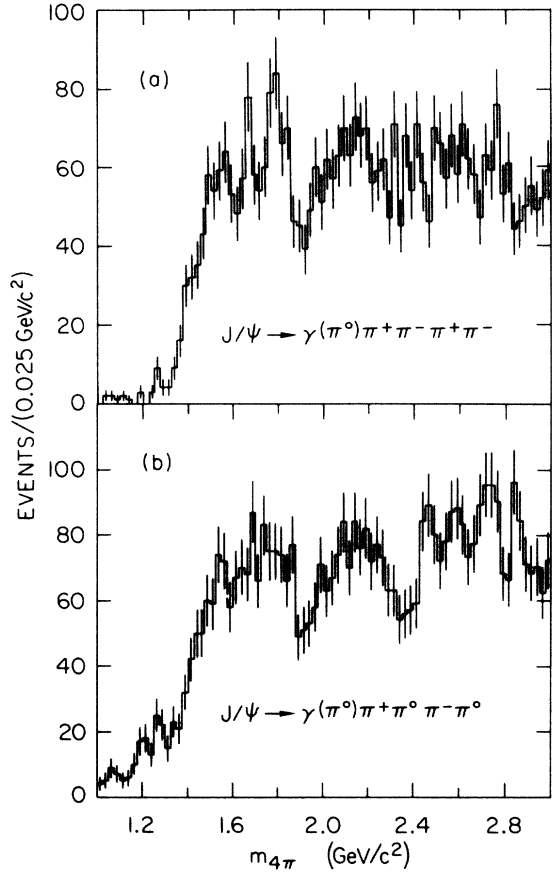


FIG. 5. $m_{4\pi}$ distributions for the event sample used in the spin-parity analyses.

taminations below $2 \text{ GeV}/c^2$ in these samples are $(11 \pm 3)\%$ for the $\gamma\pi^+\pi^-\pi^+\pi^-$ mode and between 10% and 40% in the $\gamma\pi^+\pi^0\pi^-\pi^0$ mode.

Clear $\rho\rho$ signals from the decay $J/\psi \rightarrow \gamma\rho\rho$ are evident in the $\pi\pi$ mass correlations plotted in Figs. 6(a) and 6(b). The same plots for the wrong-sign mass combinations of the four pions, Figs. 6(c) and 6(d), do not show any evidence for $\rho\rho$ enhancements. The mass combinations for the 5π event sample of Fig. 1(c) also do not exhibit enhancements in the $\rho\rho$ mass regions.

The fraction of the $\rho\rho$ component in the four-pion final state is determined using a maximum-likelihood technique. Two populations described by isotropic $\rho\rho$ and 4π phase space are assumed. The weights used in this fit are presented in the Appendix [Eqs. (A1)–(A3)]; this is the same technique used by Mark II (Ref. 7). The $\rho\rho$ distributions thus obtained are shown in Figs. 7(a) and 7(b).

We conclude, in agreement with Ref. 7, that a large fraction of the $\gamma 4\pi$ events below $2 \text{ GeV}/c^2$ is $J/\psi \rightarrow \gamma\rho\rho$. Note that the decay $J/\psi \rightarrow \pi^0\rho^0\rho^0$ would violate C -parity conservation and therefore is not a possible background; $J/\psi \rightarrow \pi^0\rho^+\rho^-$, however, is not forbidden.

III. SPIN-PARITY ANALYSIS OF THE FINAL STATE

The spin-parity of the $\rho\rho$ system is examined using two approaches. A decay-plane analysis is performed using

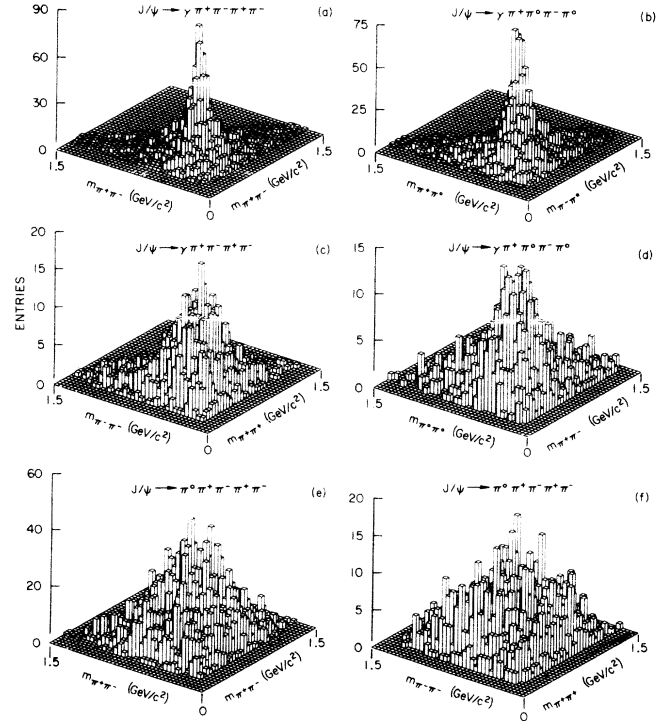


FIG. 6. Two-dimensional histograms of (a) $m_{\pi^+\pi^-}$ vs $m_{\pi^+\pi^-}$ and (b) $m_{\pi^+\pi^0}$ vs $m_{\pi^-\pi^0}$ with two entries per event; (c) $m_{\pi^+\pi^+}$ vs $m_{\pi^-\pi^-}$, and (d) $m_{\pi^+\pi^-}$ vs $m_{\pi^0\pi^0}$ with one entry per event; (e), (f) opposite- and equal-sign mass combinations for 5π events.

the $\gamma\pi^+\pi^-\pi^+\pi^-$ final state only. Then a full multichannel likelihood fit using both final states is presented.

A. Decay-plane analysis

A complete description of the final state resulting from the sequence $e^+e^- \rightarrow J/\psi \rightarrow \gamma\rho\rho \rightarrow 4\pi$ requires, for unpolarized beams, seven angles and two $\pi\pi$ submasses. The angles providing the greatest sensitivity to the spin and parity of the $\rho\rho$ system are the polar angles of the pions in their respective ρ helicity frames and χ , the sum of the azimuthal angles of the pions from the respective ρ decays, measured in the $\rho\rho$ center-of-mass system. It was pointed out by Chang and Nelson¹⁶ and Trueman¹⁷ that for decays into two vector mesons, the angle χ between the ρ decay planes provides a unique signature for even spin and odd parity, in analogy with Yang's parity test for the π^0 (Ref. 18). We have previously used this method to determine the spin-parity of the η_c using the decay into $\phi\phi$ (Ref. 19). The present analysis, however, differs in that there are two possible $\rho\rho$ combinations per event (and two χ angles) with potential interference effects, and that the event sample is not background-free. For a $\rho\rho$ sample of unique spin-parity and free of background, the distribution of χ takes the form

$$dN/d\chi = 1 + \beta \cos(2\chi),$$

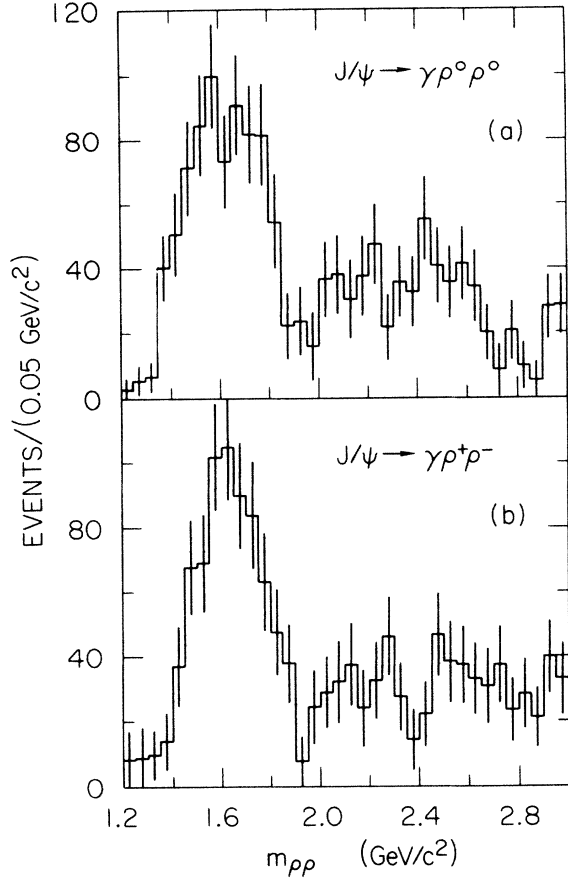


FIG. 7. Mass distributions of the $\rho\rho$ component of (a) $J/\psi \rightarrow \gamma \pi^+ \pi^- \pi^+ \pi^-$ and (b) $J/\psi \rightarrow \gamma \pi^+ \pi^0 \pi^- \pi^0$ events as determined from a two-channel fit.

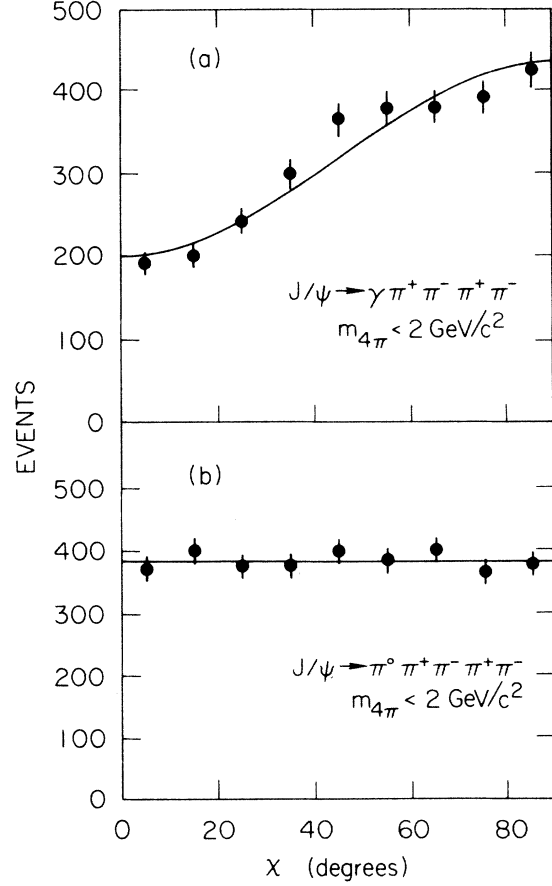


FIG. 8. Distributions of χ , the angle between the ρ decay planes, for (a) $J/\psi \rightarrow \gamma \pi^+ \pi^- \pi^+ \pi^-$ events with $m_{4\pi} < 2 \text{ GeV}/c^2$ and for (b) events from $J/\psi \rightarrow 5\pi$. The curve in (a) is a fit with $a + b \sin^2\chi$ and in (b) a fit with a constant.

where β is a constant which depends only on the spin-parity of the $\rho\rho$ system and is independent of its polarization. This is true for either $\rho\rho$ combination. Values of β are given in Ref. 19 for the lowest allowed values of the relative orbital angular momentum of the $\rho\rho$ system, $L_{\rho\rho}$; β is zero for odd spin and nonzero for even spin and its sign is the parity of the $\rho\rho$ system. In particular, for $J^P=0^-$, β is -1 , i.e., $dN/d\chi \propto \sin^2\chi$ with the two ρ 's in a relative P wave, while for $J^P=2^-$, β is -0.4 , if $L_{\rho\rho}=1$.

Figures 8(a) and 8(b) show the distribution of χ for $\pi^+ \pi^- \pi^+ \pi^-$ masses less than $2 \text{ GeV}/c^2$, for events from the $\gamma \pi^+ \pi^- \pi^+ \pi^-$ and 5π samples, respectively, with two entries per event. Figure 8(a) shows the presence of a strong $\sin^2\chi$ component in the χ distribution giving evidence for even spin and odd parity. In contrast, the background distribution shown in Fig. 8(b) is flat. As shown later, the only significant contribution of this type is $J^P=0^-$. This suggests describing the χ distribution in Fig. 8(a) by the sum of a $\sin^2\chi$ and a flat contribution. The solid curve in Fig. 8(a) shows the result of a fit with $a + b \sin^2\chi$. Defining $\alpha = b/(2a + b)$, we obtain $\alpha = 0.37 \pm 0.03$ which can be interpreted as the pseudoscalar fraction of $\gamma 4\pi$ and background events below $2 \text{ GeV}/c^2$.

The $m_{4\pi}$ dependence of α is determined by fitting the χ distribution in slices of $100 \text{ MeV}/c^2$ in $m_{4\pi}$. Figure 9(a) displays the results of these fits showing the $\sin^2\chi$ fraction for each mass bin. This fraction amounts to $\sim 50\%$ for masses between 1.5 and $2.0 \text{ GeV}/c^2$ except for a drop to $\sim 20\%$ at $1.8 \text{ GeV}/c^2$. Note that this is the mass value of the second peak in Fig. 3. The high value of $\sin^2\chi$ in the mass bin from 2.9 to $3.0 \text{ GeV}/c^2$ is consistent with the expected number of events from the decay $\eta_c \rightarrow 4\pi$ (Ref. 14). The same fit procedure, when applied to the 5π sample [Fig. 9(b)] yields a $\sin^2\chi$ contribution consistent with zero. Figure 9(c) shows the number of events attributed to the flat component obtained from the fit, i.e., $(1 - \alpha)$ multiplied by the measured four-pion mass distribution for the events of Fig. 5(a). Structure is indicated in this distribution around $1.8 \text{ GeV}/c^2$. More statistics are required to decide whether additional resonance production or a statistical fluctuation is its origin. The contribution from 5π events to this flat component is indicated by the curve whose absolute normalization is uncertain by $\sim 30\%$. The remainder is the radiative $\gamma 4\pi$ component which has a flat χ distribution. We conclude that there is a large even-spin, odd-parity $\rho\rho$ component below $2 \text{ GeV}/c^2$.

B. Multichannel spin-parity analysis

The multichannel-likelihood technique is employed to use all of the information contained in the $\gamma 4\pi$ final state. The complete formalism is described in the Appendix. Briefly, each event in a given $m_{4\pi}$ mass range is assigned a weight for each of ten hypotheses: isotropic $\rho\rho$, by which we mean $J/\psi \rightarrow \gamma\rho\rho$ without taking into account angular correlations, $\rho\pi\pi$ and 4π , also without angular correlations, and six channels for $J/\psi \rightarrow \gamma X, X \rightarrow \rho\rho$ with spin-parity $0^\pm, 1^\pm$, and 2^\pm . An $A_2\pi$ channel is also included to account for possible feedthrough from $J/\psi \rightarrow A_2\rho, A_2 \rightarrow \rho\pi$. This channel also absorbs possible contributions from $J/\psi \rightarrow \gamma A_1\pi$. The weights are nor-

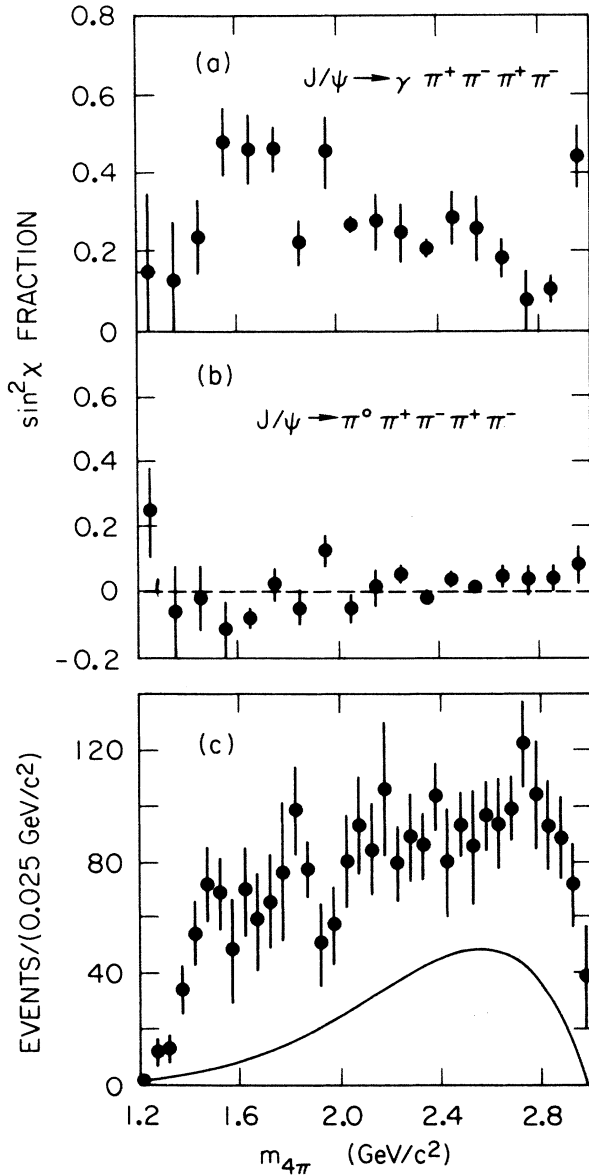


FIG. 9. Results of fits to the χ angle distribution as a function of $m_{4\pi}$: (a) the $\sin^2\chi$ fraction for $J/\psi \rightarrow \gamma 4\pi$ candidate events, (b) the $\sin^2\chi$ fraction for $J/\psi \rightarrow 5\pi$ events, (c) the flat component $(1-a)$ multiplied by the four-pion mass distribution. The solid curve in (c) shows the contribution from $J/\psi \rightarrow 5\pi$.

malized including the experimental acceptance. Maximizing the likelihood provides an estimate of the fraction of events from each source. A basic assumption is that the above list of channels is complete in that no significant channel has been excluded. Other assumptions reducing the number of unknowns are (a) only the lowest possible orbital angular momentum of the $\rho\rho$ system is allowed to contribute for a given spin-parity, (b) the ratios of the production helicity amplitudes, $x = A_1/A_0, y = A_2/A_0$, are assumed real, and (c) the different channels do not interfere. Restriction (a) is plausible for $\rho\rho$ masses close to the $\rho\rho$ threshold and (b) holds for other resonances produced in radiative J/ψ decays.⁵

The results of this multichannel fit are presented in Figs. 10 and 11 for $\gamma\pi^+\pi^-\pi^+\pi^-$ and $\gamma\pi^+\pi^0\pi^-\pi^0$, respectively, showing the number of events in each channel as a function of $m_{4\pi}$. The errors shown are statistical only. The most prominent channels are 4π phase space and $0^- \rho\rho$. The contributions to the other channels are generally small. The pseudoscalar component is very stable under variations of the fit assumptions. It should be pointed out that the exact knowledge of the size of the

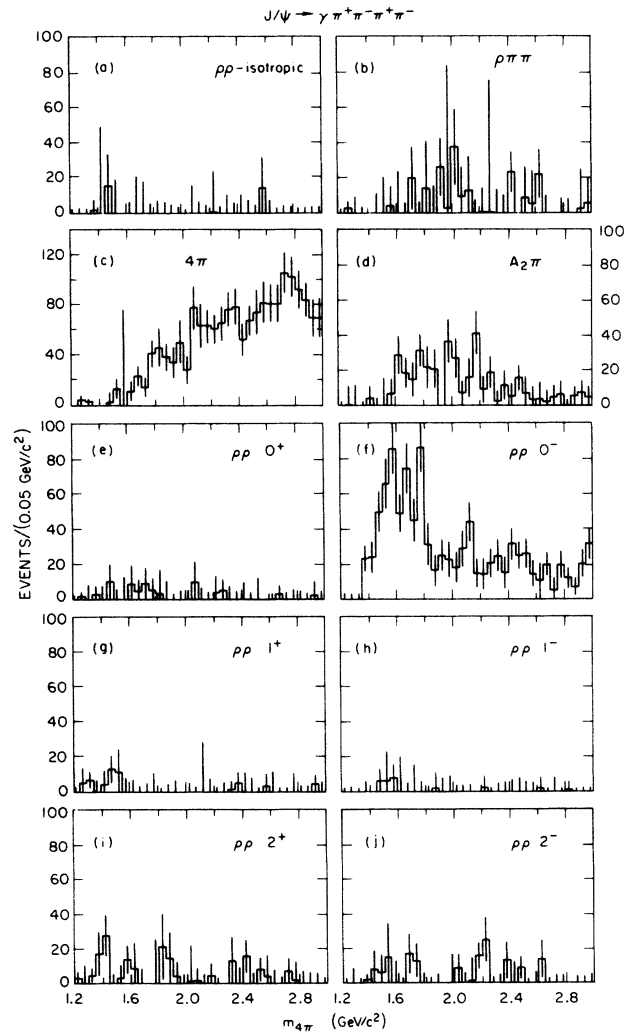


FIG. 10. Results of the channel-likelihood fits for $J/\psi \rightarrow \gamma\pi^+\pi^-\pi^+\pi^-$.

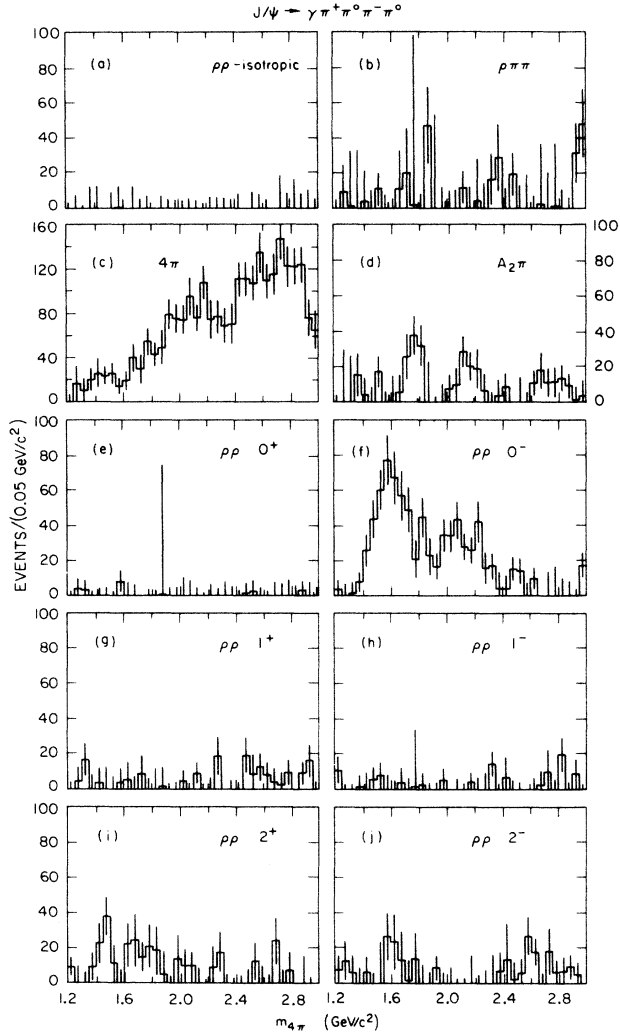


FIG. 11. Results of the channel-likelihood fits for $J/\psi \rightarrow \gamma \pi^+ \pi^0 \pi^- \pi^0$.

$J/\psi \rightarrow 5\pi$ background is unimportant for the determination of the $0^- \rho\rho$ component.

The fractions for $J^P=0^-$ are consistent with the decay-plane analysis of the previous section, showing that the $\sin^2\chi$ contribution is indeed associated with pseudoscalar $\rho\rho$. The pseudoscalar component drops off at $1.8 \text{ GeV}/c^2$. Cross checks are performed by applying the same procedure to Monte Carlo event samples and using $J/\psi \rightarrow 5\pi$ events. The latter are displayed in Fig. 12 where no significant 0^- component is found. The events mainly populate the 4π phase-space channel [Fig. 12(c)]. There are small contributions found in the $\rho\pi\pi$ and $A_2\pi$ channels, but no significant contribution in any $\rho\rho$ channel.

In Fig. 13 the events with $m_{4\pi} < 2 \text{ GeV}/c^2$ are compared with Monte Carlo calculations for various spin hypotheses in the three angles, $\cos\theta_\gamma$, the polar angle of the radiative photon in the J/ψ rest frame, $\cos\theta_\pi^*$ the pion polar angle in the ρ helicity frame, and the χ angle. The curves represent Monte Carlo simulations mixing in equal proportions isotropic 4π with $\rho\rho$ spin-parities

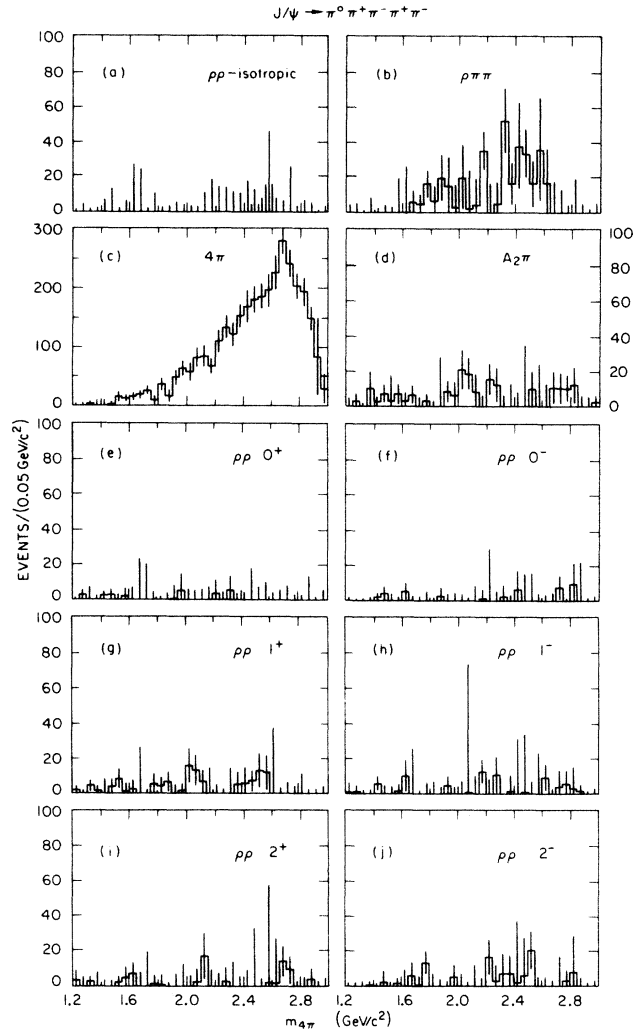


FIG. 12. Results of the channel-likelihood fits for $J/\psi \rightarrow \pi^0 \pi^+ \pi^- \pi^+ \pi^-$ background events.

$0^+, 0^-, 2^+, 2^-$. For the spin-2 simulations the relative helicity amplitude ratios x and y have been chosen to be $x=y=1$, i.e., equal amounts of helicities 0, 1, and 2.

The fraction of events from $\gamma 4\pi$ and 5π background that are due to $0^- \rho\rho$ [Fig. 10(f)] is obtained from the fit to be $(46 \pm 8)\%$ below $2 \text{ GeV}/c^2$ decreasing to about 20% above $2 \text{ GeV}/c^2$. The $(46 \pm 8)\%$ is consistent with the $(37 \pm 3)\%$ from the decay-plane analysis. Correcting for the 5π background, which is $(11 \pm 3)\%$ below $2 \text{ GeV}/c^2$, the $0^- \rho\rho$ contribution to radiative $\gamma 4\pi$ is $(51 \pm 9)\%$. Summing the $\rho\rho$ contributions to the individual spin-parity channels the fraction of $\rho\rho$ events that have 0^- spin-parity is $(76 \pm 11)\%$ below $2 \text{ GeV}/c^2$. It is interesting to note that the strong pseudoscalar $\rho\rho$ component has a counterpart in the decay $J/\psi \rightarrow \gamma \omega \omega$, where a strong $J^P=0^- \omega\omega$ component is also observed in the same mass region.²⁰

IV. DISCUSSION OF RESULTS AND CONCLUSIONS

In Sec. II evidence was presented for the radiative decay $J/\psi \rightarrow \gamma 4\pi$ in modes with two and four charged pions.

The 4π mass spectrum extends from 1.0 to 3.0 GeV/c^2 , showing peaks at 1.55 and 1.8 GeV/c^2 both about 0.1 GeV/c^2 wide. A large $\rho\rho$ component is found at 4π masses below 2 GeV/c^2 . The multichannel spin-parity analysis establishes that this $\rho\rho$ component is predominantly $J^P=0^-$ and amounts to $(51\pm 9)\%$ of the radiative $\gamma 4\pi$. The product branching fraction for pseudoscalar $\rho\rho$ is

$$B(J/\psi \rightarrow \gamma X_{0^-}) B(X_{0^-} \rightarrow \rho\rho) = (4.7 \pm 0.3 \pm 0.9) \times 10^{-3},$$

which is obtained from the $\rho^0\rho^0$ mode correcting for isospin.

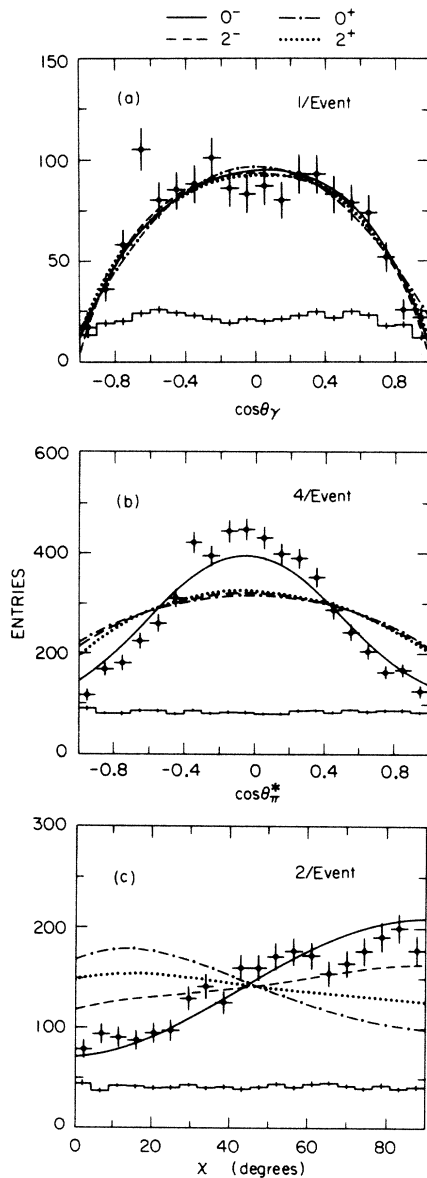


FIG. 13. Comparison of data (crosses) and Monte Carlo simulations for 0^+ , 0^- , 2^+ , and 2^- in (a) $\cos\theta_\gamma$, (b) $\cos\theta_\pi^*$, and (c) the χ angle, for events with $m_{4\pi} < 2 \text{ GeV}/c^2$. The spin-parity Monte Carlo calculations are mixed with a 50% isotropic component for the background. The histogram shows the distribution for $J/\psi \rightarrow 5\pi$ events.

The spin-parity analysis cannot unambiguously identify both peaks with pseudoscalar $\rho\rho$. The $0^- \rho\rho$ mass distribution, Figs. 10(f) and 11(f), although not inconsistent in shape with a two-peak structure, does not exhibit two clear peaks and decreases at the location of the second peak at 1.8 GeV/c^2 . Moreover, the remaining radiative component, which is the part above the curve in Fig. 9(c), is not clearly associated with any single other channel in the multichannel fit. The distribution of this component is inconsistent with $J/\psi \rightarrow \gamma 4\pi$ phase space and shows an indication of structure around 1.8 GeV/c^2 .

Achasov and Shestakov²¹ have suggested, based on a preliminary version of these results,²² that the pseudoscalar $\rho\rho$ component can be accounted for by the $\iota(1440)$, interfering with the tail of the η' and distorted by phase space and P -wave factors. Our best estimate for the pseudoscalar $\rho\rho$ component, which is an average of Figs. 10(f) and 11(f), is shown in Fig. 14 superimposed with the $\gamma 4\pi$ phase space weighted by ρ Breit-Wigner and P -wave factors (solid curve). The ratio between the data and the phase-space prediction is proportional to the matrix element squared, and is largest in the 1.4–1.5- GeV/c^2 region, supporting the suggestion of Ref. 21. A comparison of our results for the final states $\gamma K\bar{K}\pi$, $\gamma\rho\rho$, and $\gamma\omega\omega$ (Refs. 3 and 20), all of which appear to be pseudoscalar, and also $\gamma\gamma\rho$ (Ref. 23), has been performed²⁴ to test the consistency of the data with this model.

While the $\iota(1440)$ could account for at least part of the structures reported here, other plausible assignments are the radial excitations of the η and the η' (Ref. 25), both of which are expected in the mass region between 1.3 GeV/c^2 and $\sim 2 \text{ GeV}/c^2$.

The first observation of structure in $J/\psi \rightarrow \gamma\rho\rho$ gave rise to speculations that this might be a large decay mode of the $\theta(1690)$. This interpretation is ruled out by the analysis presented here. We determine the 90%-C.L. upper limits for the $\theta(1690)$ and the g_T states⁴

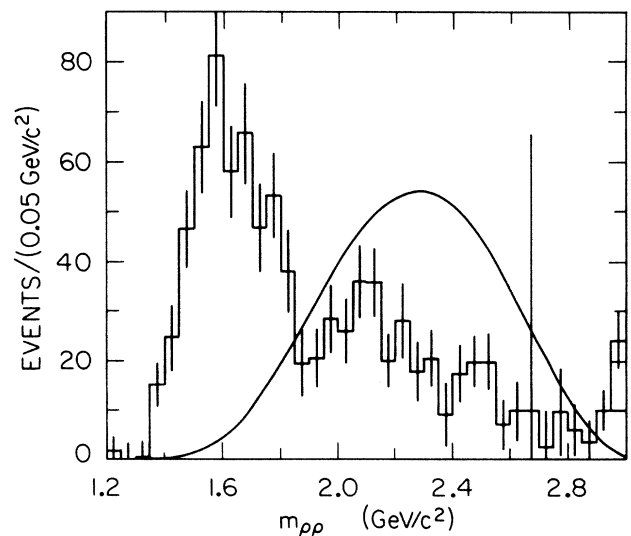


FIG. 14. Mass distribution of the pseudoscalar $\rho\rho$ component. The solid curve displays P -wave phase space for $J/\psi \rightarrow \gamma\rho\rho$.

$$B(J/\psi \rightarrow \gamma \theta) B(\theta \rightarrow \rho \rho) < 5.5 \times 10^{-4},$$

$$B(J/\psi \rightarrow \gamma g_T) B(g_T \rightarrow \rho \rho) < 6.0 \times 10^{-4}.$$

These limits are obtained from the contributions to the 2^+ channel in the mass regions $1.6\text{--}1.85 \text{ GeV}/c^2$ for the $\theta(1690)$ and $2.1\text{--}2.4 \text{ GeV}/c^2$ for the g_T states, omitting from the fit the 1^\pm and 2^- channels.

ACKNOWLEDGMENTS

We gratefully acknowledge the dedicated support of SLAC's SPEAR and Linear Accelerator operating staff. We would also like to thank the technical and engineering staffs of Group D at SLAC and the collaborating universities. One of us (N.W.) would like to thank the Alexander von Humboldt foundation for support. This work was supported in part by the Department of Energy, Contract Nos. DE-AC03-76SF00515, DE-AC02-76ER01195, DE-AC03-81ER40050, DE-AM03-76SF00034, and by the National Science Foundation.

APPENDIX: THE SPIN-PARITY ANALYSIS METHOD

Here we present details of the channel-likelihood method which is used to obtain the results in Sec. III.

The final-state pions are labeled such that 1 and 3 have the same charge, so that possible pairings to form ρ 's are (12)(34) and (14)(32). Any amplitude must be symmetric under the interchange of 1 and 3. Using this ordering, the $\gamma 4\pi$ final state can be represented by nine variables in addition to $m_{4\pi}$: m_{12}, m_{34} , the masses of the (12) and (34) pairs; θ_γ , the polar angle of the photon in the laboratory; θ_ρ and ϕ_ρ , the polar and azimuthal angles of the (12) system in the 4π helicity frame; and $\theta_1, \phi_1, \theta_3, \phi_3$, the polar and the azimuthal angles of pion 1 and pion 3 in the (12) and (34) helicity frames.

For each hypothetical channel, a weight is determined that reflects the probability to find an event with the particular final-state configuration. The different weights for each channel must be normalized properly. Let ξ represent the set of the nine variables discussed above. Then, if $g_j(\xi)$ is the amplitude for configuration ξ and channel j , the weight $w_j(\xi)$ is defined by

$$w_j(\xi) = \frac{|g_j(\xi)|^2}{\int d\xi A(\xi) |g_j(\xi)|^2}, \quad (\text{A1})$$

where $d\xi$ is the Lorentz-invariant phase-space element and $A(\xi)$ is the experimental acceptance and efficiency. Note that $d\xi$ is also invariant under exchange of any pair of final-state pions. With this normalization convention, the amplitude for 4π phase space is a constant: $g_{4\pi} = 1$. The likelihood function is then given by

$$\ln L = \sum_{i=1}^{N_{\text{ev}}} \ln \sum_{j=1}^{N_{\text{ch}}} \lambda_j w_j(\xi_i) - N_{\text{ev}} \sum_{j=1}^{N_{\text{ch}}} \lambda_j, \quad (\text{A2})$$

which is maximized varying the channel fractions λ_j and

$$\begin{aligned} \sum |T_{m\lambda}|^2 = & (1 + \cos^2\theta_\gamma) |F_0|^2 - x\sqrt{2} \cos\theta_\gamma \sin\theta_\gamma \text{Re}[F_0(F_1^* - F_{-1}^*)] + x^2 \sin^2\theta_\gamma (|F_1|^2 + |F_{-1}|^2) \\ & + y \sin^2\theta_\gamma \text{Re}(F_0(F_2^* + F_{-2}^*)) + xy\sqrt{2} \sin\theta_\gamma \cos\theta_\gamma \text{Re}(F_1 F_2^* - F_{-1} F_{-2}^*) + y^2 \frac{1}{2} (1 + \cos^2\theta_\gamma) (|F_2|^2 + |F_{-2}|^2). \end{aligned} \quad (\text{A8})$$

any other parameters on which the w_j may depend, in particular the helicity ratios x and y defined below. N_{ev} and N_{ch} denote the number of events and the number of channels, respectively.

The amplitudes which do not involve angular correlations are products and sums of appropriate Breit-Wigner factors. For $\rho\rho$, $\rho\pi\pi$, and $A_2\pi$ the expressions are

$$g_{\rho\rho} = \frac{1}{\sqrt{2}} [B_\rho(m_{12})B_\rho(m_{34}) + B_\rho(m_{14})B_\rho(m_{23})], \quad (\text{A3})$$

$$g_{\rho\pi\pi} = \frac{1}{2} [B_\rho(m_{12}) + B_\rho(m_{34}) + B_\rho(m_{14}) + B_\rho(m_{23})], \quad (\text{A4})$$

$$\begin{aligned} g_{A_2\pi} = & \frac{1}{\sqrt{8}} \{ B_\rho(m_{12}) [B_{A_2}(m_{123}) + B_{A_2}(m_{124})] \\ & + B_\rho(m_{34}) [B_{A_2}(m_{341}) + B_{A_2}(m_{342})] \\ & + B_\rho(m_{14}) [B_{A_2}(m_{142}) + B_{A_2}(m_{143})] \\ & + B_\rho(m_{23}) [B_{A_2}(m_{231}) + B_{A_2}(m_{234})] \}, \end{aligned} \quad (\text{A5})$$

where $B_\rho(m_{ij})$ denotes the relativistic ρ Breit-Wigner amplitude for $\pi\pi$ combination i,j (Ref. 26)

$$B_\rho(m) = \frac{(m_\rho \Gamma_\rho m / \rho^*)^{1/2}}{\pi(m_\rho^2 - m^2 - im_\rho \Gamma_\rho)}, \quad (\text{A6})$$

where

$$\Gamma_\rho = \Gamma_0 \left[\frac{p^*}{p_0^*} \right]^3 \frac{2p_0^{*2}}{p_0^{*2} + p^{*2}}, \quad \Gamma_0 = 155 \text{ MeV},$$

and

$$p^* = \frac{1}{2}(m^2 - 4m_\pi^2)^{1/2}, \quad p_0^* = \frac{1}{2}(m_\rho^2 - 4m_\pi^2)^{1/2}.$$

$B_{A_2}(m_{ijk})$ is defined similarly.

The helicity formalism²⁷ is used to represent $\gamma\rho\rho$ final states with a given $\rho\rho$ spin-parity. The amplitude for the decay $J/\psi \rightarrow \gamma X, X \rightarrow \rho\rho, \rho \rightarrow \pi\pi$ for a state X with spin-parity J^P is given by

$$\begin{aligned} T_{m\lambda} = & \pm \left[A_0 \frac{m + \lambda \cos\theta_\gamma}{2} F_0 - A_1 \frac{\sin\theta_\gamma}{\sqrt{2}} F_\lambda \right. \\ & \left. + A_2 \frac{m - \lambda \cos\theta_\gamma}{2} F_{2\lambda} \right], \end{aligned} \quad (\text{A7})$$

where $m = \pm 1$ and $\lambda = \pm 1$ are the ψ polarization and the γ helicity, respectively. $A_\mu, \mu \leq \min\{2, J\}$, are the unknown amplitudes for production of the state X with helicity μ , and F_μ is a function of the pion variables, given below, for its decay. Squaring (A7) and introducing $x = A_1/A_0$ and $y = A_2/A_0$, which are assumed to be real, the rate, or unnormalized weight is

The decay amplitudes F_μ are given by

$$F_\mu = B_\rho(m_{12})B_\rho(m_{34})[Q_\rho(m_{4\pi}, m_{12}, m_{34})]^L \\ \times \sum_{i,j=-1}^1 C_{ij} D_{i,0}^1(\Omega_1) D_{j,0}^1(\Omega_3) D_{\mu,i-j}^J(\Omega_\rho) + (1 \leftrightarrow 3) \quad (\text{A9})$$

with rotation matrices

$$D_{\mu,\nu}^J(\Omega) = d_{\mu,\nu}^J(\theta) e^{-i(\mu-\nu)\phi}$$

and ρ center-of-mass momentum

$$Q_\rho(m, m_1, m_2) = \{[m^2 - (m_1 + m_2)^2] \\ \times [m^2 - (m_1 - m_2)^2] / 4m^2\}^{1/2}.$$

L is the angular momentum between the two ρ 's. The notation $(1 \leftrightarrow 3)$ represents symmetrization with respect to the interchange of pions 1 and 3, and C_{ij} are decay helicity

amplitudes which are given by products of Clebsch-Gordan coefficients when projecting onto the LS basis.²⁷

For $J^P = 0^-$, (A9) can be written as

$$F_0 = [\tilde{B}_\rho(m_{12})\tilde{B}_\rho(m_{34}) - \tilde{B}_\rho(m_{14})\tilde{B}_\rho(m_{23})] \\ \times p^*(m_{12})p^*(m_{34})Q_\rho(m_{4\pi}, m_{12}, m_{34}) \\ \times \sin\theta_1 \sin\theta_3 \sin(\phi_1 + \phi_3), \quad (\text{A10})$$

where

$$\tilde{B}_\rho(m) = B_\rho(m) / p^*(m)$$

and

$$p^*(m) = (m^2/4 - m_\pi^2)^{1/2}.$$

In (A10) the sum of azimuthal angles, $\phi_1 + \phi_2$, defines the orientation between the ρ decay planes and is denoted as the χ angle in Sec. III. Note the relative minus sign between the $\rho\rho$ Breit-Wigner amplitudes required for $J^P = 0^-$, which is not obvious in (A9).

^(a)Present address: Physics Dept., University of Utah, Salt Lake City, UT 84112.

^(b)Present address: CERN, EP, 1211 Geneva 23, Switzerland.

^(c)Present address: SLAC, Stanford, CA 94305.

^(d)Present address: Lockheed Missiles and Space, Sunnyvale, CA 94086.

^(e)Present address: Anadrill/Schlumberger, Sugarland, Texas 77478.

^(f)Present address: ESL, Sunnyvale, CA 94088-3510.

^(g)Present address: Institute of High Energy Physics, Beijing, China.

^(h)Present address: ORSAY, LAL, France.

⁽ⁱ⁾Present address: Lockheed Research, Palo Alto, CA 94302.

^(j)Present address: Physics Dept., KEK Tsukuba, Ibaraki 305, Japan.

^(k)On leave of absence from University of Pisa, Pisa, Italy.

^(l)Present address: Physics Dept., Northeastern University, Boston, MA 02115.

¹M. Chanowitz, Phys. Rev. D **12**, 918 (1975); T. Appelquist *et al.*, Phys. Rev. Lett. **34**, 365 (1975); T. Appelquist, R. M. Barnett, and K. Lane, Ann. Rev. Nucl. Sci. **28**, 387 (1978).

²D. L. Scharre *et al.*, Phys. Lett. **97B**, 329 (1980); C. Edwards *et al.*, Phys. Rev. Lett. **49**, 259 (1982).

³R. M. Baltrusaitis *et al.*, Report No. SLAC-PUB-3721, 1985 (unpublished).

⁴C. Edwards *et al.*, Phys. Rev. Lett. **48**, 458 (1982).

⁵R. M. Baltrusaitis *et al.*, Report No. SLAC-PUB-3720, 1985 (unpublished).

⁶A. Etkin *et al.*, Phys. Rev. Lett. **49**, 1620 (1982).

⁷D. L. Burke *et al.*, Phys. Rev. Lett. **49**, 632 (1982).

⁸M. S. Chanowitz, in *Multiparticle Dynamics, 1983*, proceedings of the XIVth International Conference, Lake Tahoe, edited by J. F. Gunion and P. M. Yager (World Scientific, Singapore, 1983); J. F. Donoghue, in *Proceedings of the XXIth International Conference on High Energy Physics, Paris, 1982*, edited by P. Petiau and M. Porneuf [J. Phys. (Paris) Colloq. **43**, C3

(1982)].

⁹A. Bettini *et al.*, Nuovo Cimento **42**, 695 (1966); H. Bruan *et al.*, Nucl. Phys. **B30**, 213 (1971).

¹⁰R. Brandelik *et al.*, Phys. Lett. **97B**, 448 (1980); D. L. Burke *et al.*, *ibid.* **103B**, 153 (1981); H. J. Behrend *et al.*, Z. Phys. C **21**, 205 (1984).

¹¹B. A. Li, and K. F. Liu, Phys. Rev. D **30**, 613 (1984); Phys. Lett. **134B**, 128 (1984).

¹²M. Althoff *et al.*, Z. Phys. C **16**, 13 (1982).

¹³D. Bernstein *et al.*, Nucl. Instrum. Methods **226**, 301 (1984).

¹⁴R. M. Baltrusaitis *et al.*, Phys. Rev. D **33**, 629 (1986).

¹⁵This technique was first employed by T. Himel *et al.*, Phys. Rev. Lett. **45**, 1146 (1980).

¹⁶N. P. Chang and C. T. Nelson, Phys. Rev. Lett. **40**, 1617 (1978).

¹⁷T. L. Trueman, Phys. Rev. D **18**, 3423 (1978).

¹⁸C. N. Yang, Phys. Rev. **77**, 722 (1950).

¹⁹R. M. Baltrusaitis *et al.*, Phys. Rev. Lett. **52**, 2126 (1984).

²⁰R. M. Baltrusaitis *et al.*, Phys. Rev. Lett. **55**, 1723 (1985).

²¹N. N. Achasov and G. N. Shestakov, Phys. Lett. **156B**, 434 (1985).

²²N. Vermes, in *New Particle Production*, proceedings of the XIXth Rencontre de Moriond, La Plagne, France, 1984, edited by J. Tran Thanh Van (Editions Frontières, Gif-sur-Yvette, 1984); Report No. SLAC-PUB-3312, 1984 (unpublished).

²³R. M. Baltrusaitis *et al.*, Report No. SLAC-PUB-3718, 1985 (unpublished).

²⁴N. Vermes, in *Physics in Collision, 1985*, proceedings of the Vth International Conference, Autun, edited by B. Aubert and L. Montanet (Editions Frontières, Paris, 1985), p. 221; Report No. SLAC-PUB-3730, 1985 (unpublished).

²⁵T. Barnes and F. E. Close, Rutherford Report No. RAL-84-055, 1985 (unpublished), and references therein.

²⁶J. D. Jackson, Nuovo Cimento **34**, 1644 (1964).

²⁷M. Jacob and G. C. Wick, Ann. Phys. (N.Y.) **7**, 404 (1959).

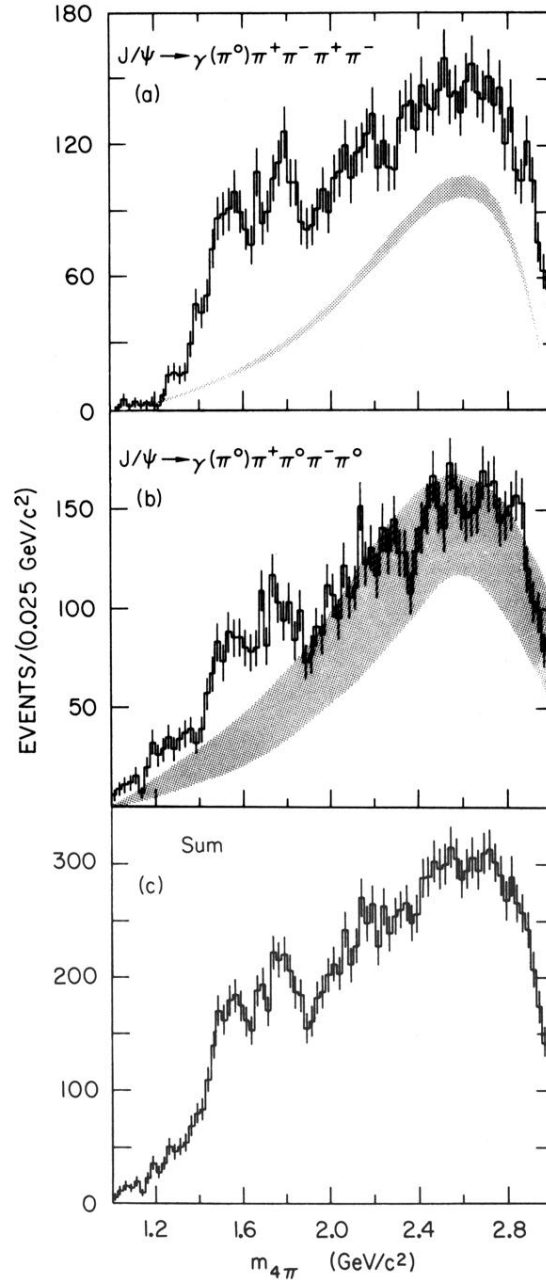


FIG. 3. $m_{4\pi}$ distributions for (a) $\pi^+\pi^-\pi^+\pi^-$ and (b) $\pi^+\pi^0\pi^-\pi^0$, for events with $p_{t,\gamma}^2 < 0.0015 \text{ (GeV}/c)^2$ (a) and $p_{t,\gamma}^2 < 0.0040 \text{ (GeV}/c)^2$ (b). The bands display the 5π background distribution estimated from Fig. 2. (c) is the sum of (a) and (b).

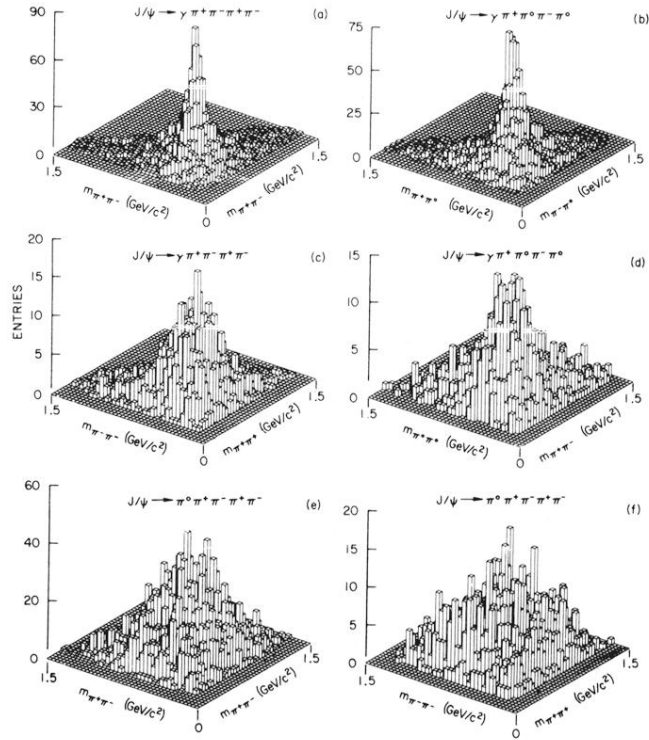


FIG. 6. Two-dimensional histograms of (a) $m_{\pi^+\pi^-}$ vs $m_{\pi^+\pi^-}$ and (b) $m_{\pi^+\pi^0}$ vs $m_{\pi^-\pi^0}$ with two entries per event; (c) $m_{\pi^+\pi^+}$ vs $m_{\pi^-\pi^-}$, and (d) $m_{\pi^+\pi^-}$ vs $m_{\pi^0\pi^0}$ with one entry per event; (e), (f) opposite- and equal-sign mass combinations for 5π events.